Study of the application of bidirectional dual active bridge converters in dc nanogrid energy storage systems

Conference Paper · October 2013

DOI: 10.1109/COBEP.2013.6785178

CITATIONS
7

READS
677

6 authors, including:

Waner Wodson Aparecido Gonçalves Silva
Universidade Federal de Itajubá (UNIFEI)
10 PUBLICATIONS **42** CITATIONS
SEE PROFILE

P.F. Donoso-Garcia
Federal University of Minas Gerais
70 PUBLICATIONS **1,210** CITATIONS
SEE PROFILE

S.I. Seleme Jr
Federal University of Minas Gerais
78 PUBLICATIONS **676** CITATIONS
SEE PROFILE

Thiago Ribeiro De Oliveira
Federal University of Minas Gerais
24 PUBLICATIONS **81** CITATIONS
SEE PROFILE

STUDY OF THE APPLICATION OF BIDIRECTIONAL DUAL ACTIVE BRIDGE CONVERTERS IN DC NANOGRID ENERGY STORAGE SYSTEMS

W. W. A. G. Silva[1], P. F. Donoso-Garcia[2], S. I. Seleme Jr.[2], T. R. Oliveira[1], C. H. G. Santos[3] and A. S. Bolzon[1]

[1]Graduate Program in Electrical Engineering - Federal University of Minas Gerais
Av. Antônio Carlos 6627, 31270-901, Belo Horizonte, MG, Brazil

[2]Department of Electronic Engineering of Federal University of Minas Gerais
Av. Antônio Carlos 6627, 31270-901, Belo Horizonte, MG, Brazil

[3]Department of Electric Engineering of Federal University of Ouro Preto
St. 37, 115, 35400-000, João Monlevade, MG, Brazil

[1]wodwaner@gmail.com, [2]pedro@cpdee.ufmg.br, [2]seleme@cpdee.ufmg.br, [1]thiago.oliveira@ifmg.edu.br,

***Abstract* – This paper discusses the application of a dual active bridge converter (DAB) as a bidirectional interface between the energy storage system and the main dc bus in a dc nanogrid. A novel control technique based on control loops competition is proposed to perform the energy management between both systems, which allows the dual active bridge to concomitantly regulate the main dc bus and control the battery bank charging process with a four states method.**

***Keywords* – Bidirectional dc-dc converter, Dual Active Bridge converter (DAB), nanogrids, microgrids, energy storage system.**

I. INTRODUCTION

Recently, due to the increasing demand on electricity consumption to meet the society needs and to address power generation deficiencies, the electric utilities are becoming more concerned in improving the supply and demand relationship through the development of the national electric grids. The great majority of the world energy demand is supplied by fossil fuels, a situation which prevents the future expansion of this energy production model due to environmental concerns about greenhouse gasses (GHG) emissions and global warming. In this juncture, the participation of renewable energy resources in the electric grid has been growing quickly in the last years. The increase of the penetration of renewable resources, known for fast dynamics and intermittent behavior, in the grid imposes new challenges for the electric utilities in terms of the need for modernization of the power generation, transmission and distribution processes, improvement of the electrical grid energy efficiency and development of new mechanisms for grid control and management that are tuned with the new requirements of this new energy system paradigm. This new concept for the electric grid is being referred as the Smart Grid [1].

The power flow in traditional power systems occurs from bulky concentrated generators to the consumers, which are connected by long transmission lines. In a Smart Grid, however, a paradigm shift is expected, in which distributed generators, based on renewable resources, will be brought closer to the consumers yielding a bidirectional power flow and which will demand also a bidirectional flow of information between the utility and the customers in order to even and control the instantaneous overall energy production and demand. Besides the environmental advantages, the Smart Grid will provide benefits for all energy conversion chain [1,2], for instance :

- Reduction of GHG emissions related to electric power generation by fossil fuels;
- Improvement in the power quality along many power levels, increasing the system stability;
- Better operational efficiency for the electric utilities, through a more active participation of the customers in the electric system;
- Greater integration of distributed generation with the electric grid by means of information technology and smart communication;
- Possibility of bidirectional power flow.

The Smart Grid introduces new concepts for the electric system, such as the microgrids and nanogrids. The microgrids are cogeneration systems based on renewable energy sources, as solar photovoltaics (PV), wind power, microturbines and fuel cells, intended to supply small sets of customers, as residential complexes, hospitals, data centers, schools, etc, [3]. The microgrid can be represented as a small independent power system, which associates local loads and distributed generation with a power capacity of 10 to 100kW [4,5]. The nanogrids can be seen as a small part of a microgrid, with a similar composition, local generation based on renewable resources and energy storage, but with a power capacity up to 25kW, intended for residential or commercial buildings purposes [3]. Figures 1 depicts this new electric system concept with distributed generation, micro and nanogrids and their interaction in a local network.

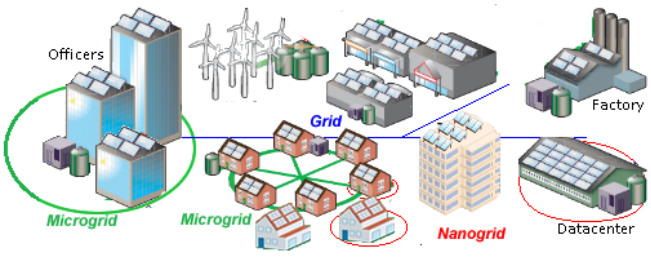

Fig. 1. Micro and nanogrid integrated with local power system.

One of the main features of the nanogrid is the ability to island itself from the electric grid during system disturbances and faults, which improve the power quality perceived by the local loads and ensure a proper autonomy for critical loads.

In order to perform this islanding process and allow a soft reconnection to the electric grid, the nanogrid must be connected to the main grid through a bidirectional converter [3]. This converter must also perform the control of the power flux and synchronize to the electric grid frequency and phase, which leads to a more complex converter architecture. An alternative to minimize the nanogrid complexity is to utilize dc-powered systems. Dc distribution systems have the advantage of enhancing the system overall efficiency, since power losses on cables are lower than in equivalent ac systems, most residential and commercial buildings loads are intrinsic dc loads, which permits the elimination of energy conversion stages and there is a better integration with renewable resources and energy storage devices [6].

A well accepted structure for a dc nanogrid is based on two main voltage levels inside the distribution system: a higher voltage dc bus of 380V and a low voltage dc bus of 48V [6]. The 380V voltage level was chosen to cope with the output voltage of typical power factor correctors (PFC) associated with electronic devices of 70W or higher. Therefore the adaption of currently electronic devices to this new dc-based voltage standard would not demand significant alterations on the devices internal design. The low voltage level of 48V meets telecommunication standards and is suitable to supply low power devices and provides a safe voltage level to be handle by the consumers [6].

In order for a nanogrid to provide uninterrupted supply of local loads, even in the event of electric grid outages and intermittent behavior of distributed generation, it is mandatory that it possess an energy storage system, normally based on batteries [7]. The interface of the main dc bus of the nanogrid and the storage system devices is performed by a dc-dc bidirectional converter which assures voltage regulation of the main dc bus whenever needed. For this work, a dual active bridge (DAB) was considered to implement the bidirectional interface between the dc bus and the storage system low voltage bus. The main features of the DAB topology are: bidirectional power flux, galvanic isolation and capacity to step-up or step-down the voltage levels of its inputs [8]. Figure 2 presents the power stage topology of the DAB converter, which consists of two H-bridges interconnected by a high frequency transformer. The leakage inductance of the transformer, represented by L, is responsible for instantaneous energy storage [9].

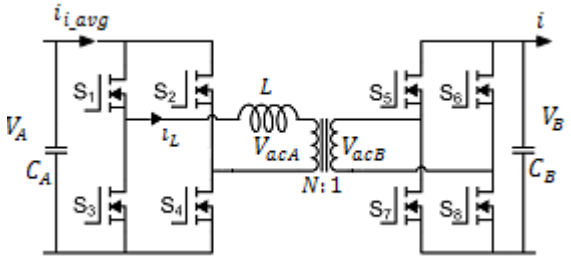

Fig. 2. DAB converter topology.

In the technical literature, several works about the operation and control of the dual active bridge converter can be found [7-17]. In [7] the DAB is immersed in a microgrid system being employed as the interface with the battery bank and its control is based on the phase-shift modulation. In [8], a nonlinear control technique for the power flux is implemented intending to regulate the converter output voltage. In [11], the modulation method is modified to control the voltage across one of the H-bridges in order for the converter to operate in a greater voltage level. In [12], a control strategy for the DAB operating as the interface converter for a battery bank is discussed, in which the bank state of charge, output current and the microgrid operation mode are taken in consideration for the controlling actions. References [13-17] address methods that improve the DAB efficiency through modulation techniques and/or non-dissipative ZVS.

This paper proposes a novel control technique for the DAB converter applied in nanogrid systems which controls the power flux between the dc bus and the battery bank, assuring a regulated dc bus voltage on the nanogrid side and respecting the charging algorithm of the battery bank. The theoretical studies will be carried out on a dc nanogrid with a 380V dc bus and a battery bank low voltage bus of 48V, as proposed in [6]. A small scale prototype was built to validate the control technique performance. This prototype operates with a 24V dc bus, on the nanogrid side, and a 12V low voltage bus on the battery side.

II. DAB CONVERTER OPERATION ANALYSIS

Each H-bridge of the DAB converter generates a 50% duty cycle square wave [10]. The control of the power flux and the amount of energy transferred by the converter is realized through the definition of the phase angle between these two square waves. This control technique is referred as phase-shift control [7]. Figure 3 shows the waveforms of the transformer primary and secondary voltages, V_{acA} and V_{acB} respectively, where T represents a complete switching period and $T_{1/2}$, a half switching cycle. Notice that V_{acA} leads V_{acB} of $d * T_{1/2}$ seconds, where $d = \emptyset/180°$ and $\emptyset \in [-180°, 180°]$ is the angular phase shift between the primary and secondary voltages. The power transfer occurs in the time interval $d * T_{1/2}$. Figure 4 shows the L inductor current waveform. Note that the time interval $d * T_{1/2}$ is divided in time periods t_1 and t_2.

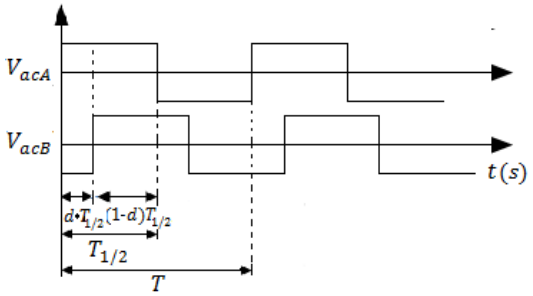

Fig. 3. DAB transformer voltage waveforms.

Assuming V_A as the nanogrid main dc bus voltage, V_B as the dc voltage across the battery bank, $V_B' = V_B N$ as the secondary side voltage reflected to transformer primary and $d * T_{1/2} = t_1 + t_2$, the following equations can be defined:

$$V_A + V_B' = L\frac{di_L}{dt} \qquad 0 \le t < d * T_{1/2} \tag{1}$$

$$V_A - V_B' = L\frac{di_L}{dt} \qquad d * T_{1/2} \le t < T_{1/2} \tag{2}$$

Solving (1) and (2), it obtains:

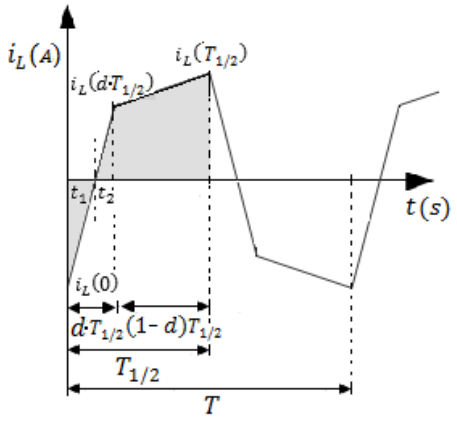

Fig. 4. Inductor current waveform (i_L).

$$i_L(t) = \frac{1}{L}\int_0^{d*T_{1/2}} V_A + V_B'\,dt \rightarrow \frac{V_A + V_B'}{L} dT_{1/2} \quad (3)$$

$$i_L(t) = \frac{1}{L}\int_{d*T_{1/2}}^{T_{1/2}} V_A - V_B'\,dt \rightarrow \frac{(V_A - V_B')(1-d)}{L} T_{1/2} \quad (4)$$

Considering $i_L(0) = -i_L(T_{1/2})$ and $i_L(t) = i_L(d * T_{1/2}) + i_L(T_{1/2})$ for $0 \le t < d * T_{1/2}$, $i_L(t) = i_L(T_{1/2}) - i_L(d * T_{1/2})$ for $d * T_{1/2} \le t < T_{1/2}$. Combining it with (3) and (4) and solving the resulted system, the following relations are achieved:

$$i_L(T_{1/2}) = \frac{(2V_B'd + V_A - V_B')T_{1/2}}{2L} \quad (5)$$

$$i_L(d * T_{1/2}) = \frac{(2V_A d - V_A + V_B')T_{1/2}}{2L} \quad (6)$$

It can be observed in Figure 4 that the triangles formed by $i_L(0)t_1$ e $i_L(d * T_{1/2})t_2$ have angles opposed by their vertices, which leads to $i_L(T_{1/2})/t_1 = i_L(d * T_{1/2})/t_2$, substituting it in (5) and (6), it obtains:

$$t_1 = T_{1/2}(2V_B'd + V_A - V_B')/(2V_B' + 2V_A) \quad (7)$$

$$t_2 = T_{1/2}(2V_A d - V_A + V_B')/(2V_B' + 2V_A) \quad (8)$$

The DAB average input current i_{i_avg} is defined by the areas under the i_L curve in time interval$T_{1/2}$, which are shown in Figure 4 as the hatched areas. The average input current is defined in (9):

$$i_{i\_avg} = \frac{1}{T_{1/2}}\left(\frac{i_L(0)t_1}{2} + \frac{i_L(d * T_{1/2})t_2}{2} \ldots + \frac{[i_L(T_{1/2}) + i_L(d * T_{1/2})](1-d)T_{1/2}}{2}\right) \quad (9)$$

Substituting (5), (6), (7) and (8) in (9), it obtains:

$$i_{i\_avg} = \frac{V'_B d * T_{1/2}(1-d)}{L} \quad (10)$$

Assuming $P = i_{i\_avg}V_A$ and $T = 2T_{1/2} = 1/f_s$ and substituting it into (10), the converter transferred power is defined as in (11):

$$P = \frac{V_A V_B N d(1-d)}{2Lf_s} \quad (11)$$

Where f_s is the converter switching frequency. Using (10) the DAB converter can be modeled as a current source. The equivalent circuit model of the DAB used in this work is presented in Figure 5. The battery is modeled as a series RC branch, where R stands for the battery internal resistance and C, for a capacitance representing the battery charge capacity. C is defined as: $C = \frac{Battery\ nominal\ capacity\ C(Ah)}{Battery\ nominal\ voltage} \times 3600$.

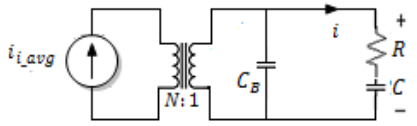

Fig. 5. Current source model for the DAB converter.

Through the converter model, the battery charging current can be defined, in Laplace domain, for the equation described in (12). The small-signal model for the DAB converter can be obtained through (12), considering for this matter $d = D + \hat{d}$ and $V_B = VB + \hat{V}_B$, where D and VB are steady state operation points and $\hat{d}$ and $\hat{V}_B$ are small-signal perturbations in the phase-shift and battery side output voltage. The output current small-signal value is defined in (13), out of which the system transfer functions are obtained and presented in (14), (15) and (16):

$$i(s) = N^2 \frac{V_B d(1-d)}{2Lf_s} \frac{sC}{s^2RCC_B + s(C + C_B)} \quad (12)$$

$$\hat{\imath}(s) = \frac{\partial i}{\partial d}\bigg|\hat{d} + \frac{\partial i}{\partial V_B}\bigg|\hat{V}_B \rightarrow G_{id}(s)\hat{d} + G_{iV_B}(s)\hat{V}_B \quad (13)$$

$$G_{id}(s) = N^2 \frac{VB(1-2D)}{2Lf_s} \frac{sC}{s^2RCC_B + s(C + C_B)} \quad (14)$$

$$G_{iV_B}(s) = N^2 \frac{D(1-D)}{2Lf_s} \frac{sC}{s^2RCC_B + s(C + C_B)} \quad (15)$$

$$G_{V_Bi}(s) = 1/G_{iV_B}(s) \quad (16)$$

Whether the power flux in the DAB converter is inverted, the converter model in relation to the battery current *i(s)* will be modified according to the model depicted in Figure 6. R_L represents the nanogrid main dc bus load, which can be estimated by $R_L = \frac{V_A^2}{P_N}$, where P_N is the power demanded by the nanogrid local load. The current source I_{bus} stands for all other power sources present in the nanogrid and can be estimated by $I_{bus} = \frac{V_A}{P_N}$. This way (17), (18), (19), (20) and (21) are obtained:

$$V_A(s) = \frac{R_L}{R_L sC_A + 1}(I_{bus} + \frac{i(s)}{N}) \quad (17)$$

$$\hat{V}_A(s) = \frac{\partial V_A}{\partial I_{bus}}\bigg|\hat{I}_{bus} + \frac{\partial V_A}{\partial i}\bigg|\hat{\imath} + \frac{\partial V_A}{\partial R_L}\bigg|\hat{R}_L \quad (18)$$

$$\frac{\partial V_A}{\partial i}\bigg|\hat{V}_A = G_{V_Ai}(s)\hat{V}_A \quad (19)$$

$$G_{V_Ai}(s) = \frac{R_L}{N(R_L sC_A + 1)} \quad (20)$$

$$G_{iV_A}(s) = 1/G_{V_Ai}(s) \quad (21)$$

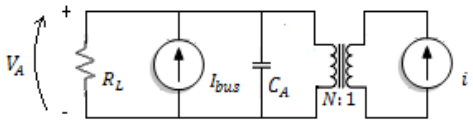

Fig. 6. DAB current source model for a power flux from the battery bank to the nanogrid dc bus.

Based on (14), (15), (16), (20) and (21), a block diagram representing the DAB converter small-signal model can be constructed. This block diagram is depicted in Figure 7.

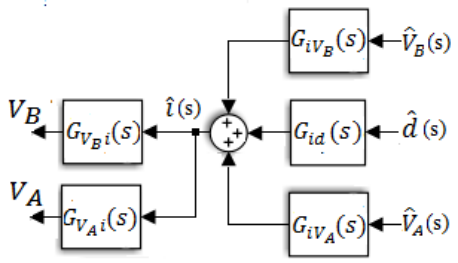

Fig. 7. DAB converter small-signal model.

III. BATTERY CHARGING PROCESS

The battery charging method considered for this work is described by the flowchart shown in Figure 8 and is named the four states algorithm. This method defines four stages for charging the battery and utilizes constant current to charge the battery cells and constant voltage to recover the battery complete capacity [18,19]. When the battery is supplying power to the system its terminal voltage decreases until it reaches the cutoff voltage (V_{off}), which represents the minimum battery terminal voltage recommended by the manufacturer. Whether the battery terminal voltage falls below the cutoff limit it will experience irreversible sulfation and its life cycle will be diminished. V_{equ} stands for the equalization voltage used to equalize the stored charge in each element of a battery bank, this voltage level is achieved at the end of a fast charging process and intermediates the transition to the fluctuation state. When in fluctuation, the batteries are completely charged and the voltage level applied in this case is

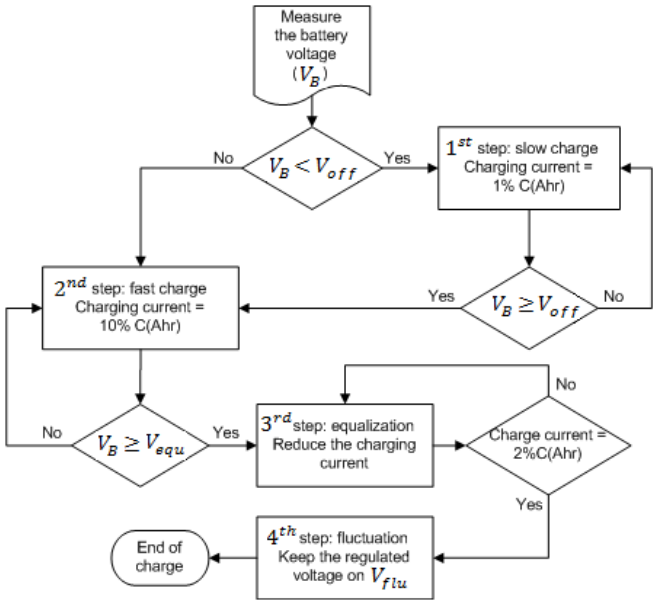

Fig. 8. Flowchart for the four state charging algorithm.

used to compensate the natural self-discharge process of the battery bank, and maintain a regulated voltage of V_{flu} across the bank. This stage is critical, since a overvoltage applied during the fluctuation state will provoke a reduction on the battery life cycle and may even unutilized it [18,19].

IV. CONVERTER CONTROL

The control strategy monitors the nanogrid dc bus voltage and when it becomes greater than 380V, the DAB converter will drain a maximum allowable current from the dc bus in order to charge the battery. However, when the bus voltage drops below 380V, the converter will gradually reduce the current value, if the dc bus still does not recover, the current direction will be changed, inverting the power flux and using the battery bank as a power source for the nanogrid system. The DAB will cease to operate in two conditions: firstly, when the dc bus voltage drops below 380V and the battery bank is already fully discharged, *i.e.*, with a terminal voltage below 43V, and secondly when the dc bus voltage is greater than 380V and the battery bank is fully charged, *i.e.*, in fluctuation state with a terminal voltage of 55.2V. The block diagram for the proposed control is shown in Figure 9. The blocks denoted by letter A refer to the nanogrid dc bus side of the DAB converter, and the ones denoted by letter B refer to the battery bank side.

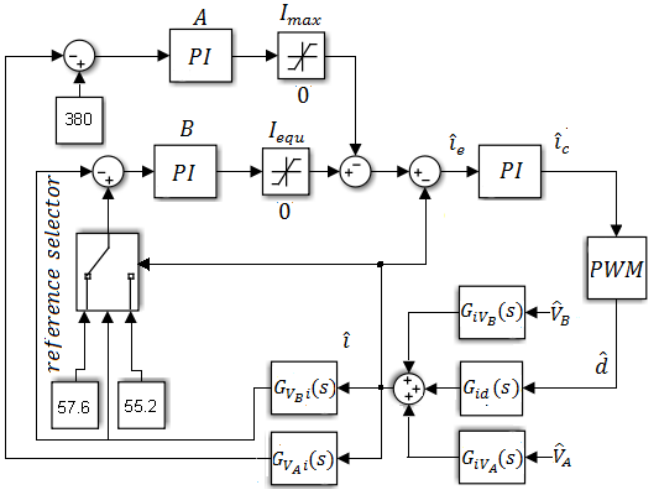

Fig. 9. Proposed control block diagram.

The control technique possesses two control loops, A and B, which control the nanogrid dc bus voltage and the battery bank terminal voltage, respectively. The output of the PI compensators define two current references for the system and the actual reference of the current loop is the difference between reference B and reference A. Notice that the current reference B saturation limit, named I_{equ}, is set to the maximum limit of the charging process which is 10% of the rated battery bank capacity. Current reference B, on the other hand, presents a saturation limit equal to I_{max}, which is defined as I_{equ} plus the maximum battery discharge current. Therefore, when the PI compensator of the loop A saturates, it will cancel the charging current imposed by the loop B and force the change of the current direction, *i.e.*, it will force the inversion of the power flux. In another words, loops A and B constantly competes to determine the power flux of the DAB converter and as a result the system energy balance is pre-

served. Notice also that the loop B has two voltage references. The first one is the equalization voltage (57.6V), which is set every time that the control system senses that the battery has been discharged, what is defined by the fact that the battery bank terminal voltage fell below 53V. The second reference is the fluctuation voltage (55.2V), which is set whenever the equalization voltage is actually reached by the battery bank.

This control structure presents advantageous features such as: soft transition between the charge and discharge processes, due to the control loops competition; automatic definition of the power flux and proper determination of the operation point only by local variables measurement and no overvoltage or overcurrent is imposed on the battery bank.

V. EXPERIMENTAL RESULTS

The experimental results were carried out on a small scale prototype, in which the nanogrid dc bus was represented by a 24V voltage source and the battery bank low voltage bus is a 12V lead-acid battery. Table I presents the DAB converter parameters, the compensators gain and the voltage and current values considered for the charging algorithm, derived from battery manufacturer's datasheet. Figure 10 presents the waveforms of the DAB converter, where channel 1 (blue) is the transformer primary voltage (V_{acA}), channel 2 (red) is the transformer secondary voltage (V_{acB}) and channel 3 (magenta) is the inductor current.

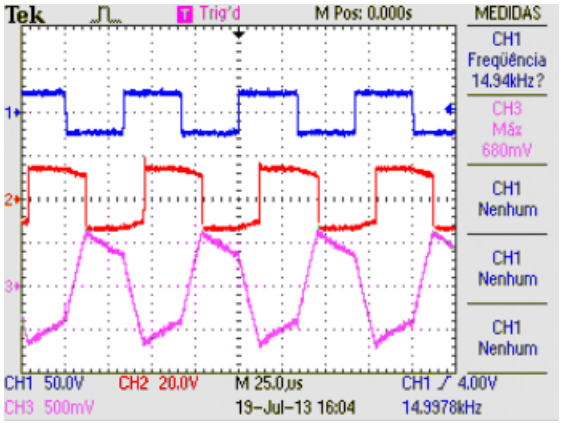

Fig. 10. DAB converter voltage and current waveforms.

Figure 11 shows the voltage and current levels on the battery during a full charge process, the values were measured with a 1 second sampling time. It can be observed three steps in the charge algorithm: *fast charge*, during the time interval between 0h and 4h, *equalization,* during the time interval between 4h and 5h30, and *fluctuation*, which occurred between 5h30 and 6h30. The maximum charging current was set to 0.9A. Through Figure 11, it can be seen that when the battery voltage reaches the equalization level (V_{equ}), the charging current decreases until it reaches 0.18A. From this point forth the voltage reference switches to the fluctuation level, in which the current delivered to the battery is small and just enough to compensate the losses produced by the battery self-discharge process.

Figure 12 illustrates the experimental results for a load perturbation on the dc bus. It can be observed that when the dc bus voltage sags, the battery charging current is gradually reduced, becoming negative, which means that the converter power flow has been inverted, and it provides enough power to regulate the dc bus to its nominal voltage. A similar process is noticed when the dc bus voltage becomes larger than 24V. It can be observed in Figure 12.c the smooth transition between charging and discharging the battery.

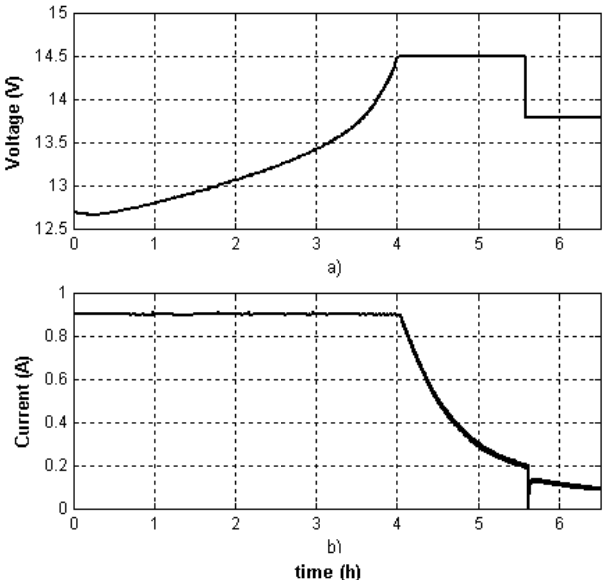

Fig. 11. Experimental results for a full charge process of the battery bank. a) Battery side output voltage. b) Charging current.

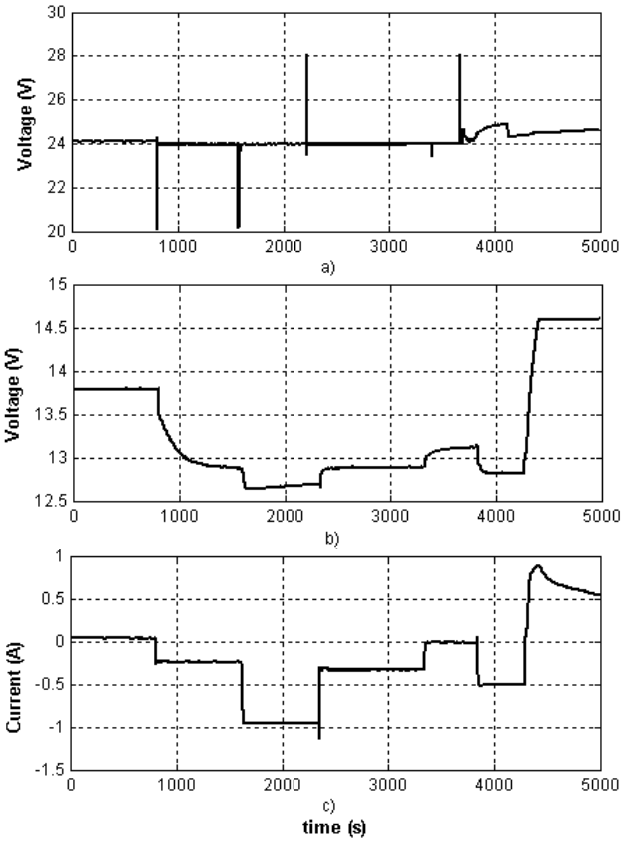

Fig. 12. Experimental results for a load perturbation in the dc bus. a) Dc bus voltage. b) Battery terminal voltage. c) Battery charging current.

TABLE I

Experimental converter parameters.

Nominal Power	15W
Transformer	N1:N2 = 2:1 L = 325µH
Battery bank	9Ahr/12V
Voltage levels ($V_{off}, V_{equ}, V_{flu}$)	10.5V, 14.5V, 13.8V
Capacitor	C_A=2200 µF, C_B=4700µF
Switching frequency	15kHz
Compensator gains.	
Compensator A	Kp=0.2 Ki=120
Compensator B	Kp=30 Ki=80
Current loop compensator	Kp=0.01 Ki=2

VI. CONCLUSION

In this paper the employment of a DAB converter as a interface between a nanogrid main dc bus and a battery bank is evaluated. A control strategy was proposed, in which the converter assures proper charging procedure for the battery bank, according to a 4-step algorithm, and regulated dc bus on the nanogrid side. Both goals are achieved by the difference between the battery side and nanogrid side control loops. Through experimental results conducted on a small scale system the behavior of the control scheme was validated. The correct following of the charging steps were observed and concomitant to it the dc bus of the nanogrid was kept around its nominal voltage. During the whole converter operation the power flow inversion occurred in smooth transitions, showing that the control technique does not produce oscillatory behavior and unpredictable situations.

ACKNOWLEDGEMENT

This work has been supported by the Brazilian agency CAPES and FAPEMIG.

REFERENCES

[1] Falcão, Djalma M. "Integração de Tecnologias para Viabilização da Smart Grid". *III Simpósio Brasileiro de Sistemas Elétricos*, pp. 1-5, 2010.

[2] S. Chowdhury, S. P. Chowdhury, P. Crossley, *Microgrids and Active Distribution Networks*, IET, 1st Edition, London, United Kingdom, 2009.

[3] Cvetkovic, I. "Modeling, Analysis and Design of Renewable Energy Nanogrid", *Dissertation of Master of Sciences*, Virginia Tech, EUA, 2010.

[4] R. H. Lasseter, P. Paigi, "Microgrid: A Conceptual Solution", *in Power Electronics Specialists Conference*, vol. 6, pp. 4285-4290, 2004.

[5] R. Lasseter, "Microgrid and Distributed Generation", *Journal of Energy Engineering, American Society of Civil Engineers*, Sep 2007.

[6] D. Boroyevich, I. Cvetkovic, D. Dong, R. Burgos, F. Wang, F. Lee, "Future electronic power distribution systems – a contemplative view", *in 12th International conference on Optimization of Electrical and Electronic Equipment (OPTIM)*, pp 1369-1380, May 2010.

[7] B. Zhao, Q. Yu, W. Sun, "Extended-Phase-Shift Control of Isolated Bidirectional DC–DC Converter for Power Distribution in Microgrid", *IEEE Transactions On Power Electronics,* vol. 27, no. 11, pp. 4667-4680, November 2012.

[8] D. D. M. Cardozo, J. C. Balda, D. Trowler, H. A. Mantooth, "Novel Nonlinear Control of Dual Active Bridge", *in Applied Power Electronics Conference and Exposition (APEC)*, pp. 321-327, 2010.

[9] M. H. Kheraluwala, R. W. Gascoigne, "Performace Characterization of a High-Power Dual Active Bridge dc-to-dc Converter", *IEEE Transactions On Industry Applications,* vol. 28, no. 6, pp. 1294-1301, November/December 1992.

[10] A. R. Alonso, D. G. Lamar, A. Vazquez, J. Sebastian, M. M. Hernando, "An overall study of a Dual Active Bridge for Bidirectional DC/DC conversion", *in Energy Conversion Congress and Exposition (ECCE)*, 2010.

[11] H. Zhou, A. M. Khambadkone, "Hybrid Modulation for Dual-Active-Bridge Bidirectional Converter With Extended Power Range for Ultracapacitor Application", *IEEE Transactions On Industry Applications,* vol. 45, no. 4, pp. 1434-1442, July/August 2009.

[12] M. A. Sofla, Lingfeng Wang, "Control of DC-DC Bidirectional Converters for Interfacing Batteries in Microgrids", *in Power Systems Conference and Exposition (PSCE),* pp. 1-6, 2011.

[13] M. Kim, M. Rosekeit, S. Sul, R. W. A. A. De Doncher, "A Dual-Phase-Shift Control Strategy for Dual-Active-Bridge DC-DC Converter in Wide Voltage Range", in *8th International Conference on Power Electronics – ECCE*, pp. 364-371, May 30-June 3 2011.

[14] G. G. Oggier, R. Leidhold, G. O. García, A. R. Oliva, J. C. Balda, F. Barlow, "Extending the ZVS Operating Range of Dual Active Bridge High-Power DC-DC Converters", *in Power Electronics Specialists Conference*, pp. 1-7, 2006.

[15] G. G. Oggier, G. O. García, A. R. Oliva, "Modulation Strategy to Operate the Dual Active Bridge DC-DC Converter Under Soft Switching in the Whole Operating Range", *IEEE Transactions On Power Electronics,* vol. 26, no. 4, pp. 1228-1236, April 2011.

[16] G. G. Oggier, G. O. García, A. R. Oliva, "Switching Control Strategy to Minimize Dual Active Bridge Converter Losses", *IEEE Transactions On Power Electronics,* vol. 24, no. 7, pp. 1026-1838, July 2009.

[17] D. Costinett, R. Zane, D. Maksimovic, "Automatic Voltage and Dead Time Control for Efficiency Optimization in a Dual Active Bridge Converter", *in Applied Power Electronics Conference and Exposition (APEC)*, pp. 1104-1111, 2012.

[18] A. Trento, A. T. Feldens, "Carregador de Baterias Tipo Chumbo Ácido com PIC16F876A", *in Toroid do Brasil, AN 08002*,vol. 1.0, S. José dos Pinhais PR Brazil, Jan/2008.

[19] Texas Instruments, "U-510 Using the bq2031 to Charge Lead-Acid Batteries", Texas Instruments Incorporated, pp. 15, 1999.

[20] F. Krismer, "Modeling and Optimization of Bidirectional Dual Active Bridge DC–DC Converter Topologies", *Dissertation of Doctor of Sciences*, ETH ZURICH, 2010.